Enhanced Piezoelectric Effects in Three-Dimensionally Coupled Self-Assembled Quantum Dot Structures

Pilkyung Moon[1], Youngsoo Lee[1], Eungjin Ahn[1], Jungsub Kim[1], Changjae Yang[1], Gun-Do Lee[1], Euijoon Yoon[1,*], and Jean-Pierre Leburton[2]

[1]Compound Semiconductor Epitaxy Laboratory, School of Materials Science and Engineering, Seoul National University, Seoul 151-742, Korea
[2]Beckman Institute for Advanced Science and Technology and Department of Electrical and Computer Engineering, University of Illinois at Urbana-Champaign, Urbana, Illinois 61801, USA

We investigated the influence of piezoelectric effects on the quantum mechanical coupling in two types of self-assembled quantum dot (QD) configurations: (i) laterally ([110]) coupled structures and (ii) anti-correlated stacked structures, by using an eight-bands **k·p** method. We show that the valence band ground state of laterally coupled quantum dots (LCQDs) is highly localized in the coupling region. Optical transitions involving such a localized state exhibit strong red shifts compared to similar transitions in single QDs. Unlike LCQDs that show symmetric coupling between the two quantum dot (QD) wave functions, QDs on the upper and lower planes of the anti-correlated structures have asymmetric configurations, therefore the coupling occurs between different states in these two planes (mixed coupling). The origin of the spectral shift in the anti-correlated structures is interpreted in terms of the strain and confinement condition in the coupled QDs.

**Keywords:** piezoelectric effect, coupled self-assembled quantum dots, k·p method, optical transitions

1. INTRODUCTION

Quantum dots (QDs) have received great interest for applications such as lasers for optical fiber communications[1], semiconductor optical amplifiers (SOA)[2], and spin filters[3]. In addition, QDs can be utilized as a key building block in solid-state quantum computing through the formation of a quantum gate[4]. QDs in such devices are characterized by the discreteness of electron energies that originates from a three-dimensional quantum mechanical confinement. The delta-function-like absorption and emission spectra in optoelectronic devices, such as LEDs, lasers and SOAs, are based on this discreteness of energy. Due to the quantized energy, only transitions having specific energies are allowed in transitions between different states. Among the possible factors affecting the electronic and optical properties of QDs are such factors as the strain, piezoelectric potential, composition profiles and the geometries of the QDs. In order to obtain desired properties, such as transitions at specific energies, it is considered necessary to tune the above parameters through trial and error. Computational simulation can provide good guidelines for such parameters, and offers rigor-

ous physical interpretations of the properties of QDs.

Figure 1(a) shows an atomic force microscopy (AFM) image of a typical InAs/GaAs QD and its photoluminescence (PL) spectra[5]. The geometry of each QD is lens-shaped with a 21.0 nm base length and a 5.41 nm height. Figure 1(b) exhibits the interband PL spectra of the QDs in Fig. 1(a). In order to investigate the strain distribution of general QDs and its influence on the PL spectra, we used valence force field method (VFF)[6,7] and eight-band k·p method[8]. Details of these methods are described in Sec. 2. In-plane strain ($e_{xx}+e_{yy}$) distribution of a single QD (SQD) is shown in Fig. 2, and it shows a good agreement with a general TEM image of QDs[9]. The interband transition energies are determined by the electron energies in the QD, and the transition strengths are calculated from their wavefunctions. Figure 3 exhibits the transition spectra of the QDs shown in Fig. 2. Each peak has a finite spectral line width due to the inhomogeneity in the size distributions of the QDs. The effects of QD geometry, size, compositional grading, and external fields to the electronic and optical properties of QDs can be obtained by the simulation[10]. In addition, more complicated structures such as QDs with an insertion layer[11] and a strain reducing layer[12] were investigated. In this manner, a computational simulation can provide a useful interpretation of the properties of QDs as well as good predictions of the
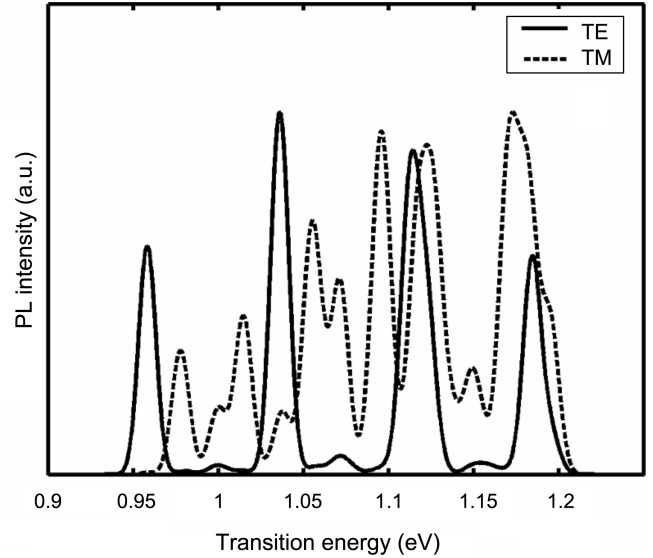
*Corresponding author: eyoon@snu.ac.kr
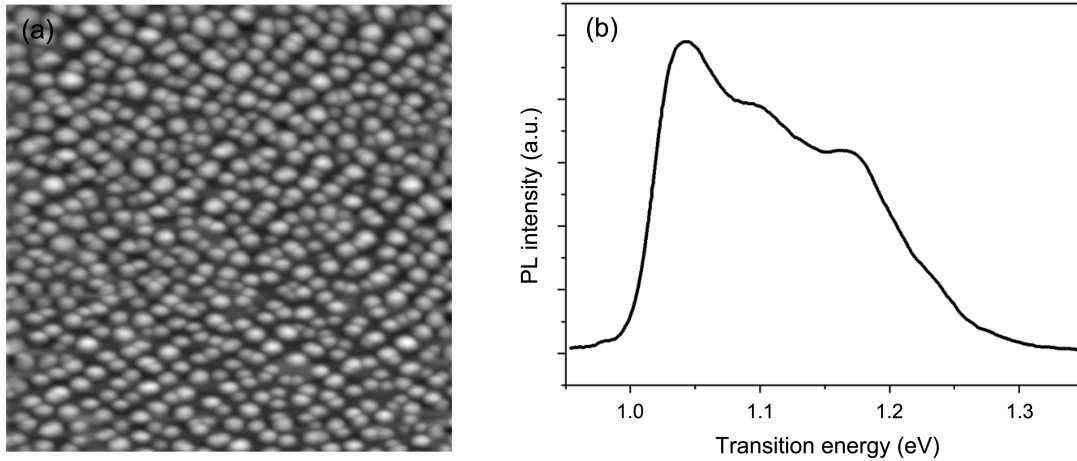
Fig. 1. An InAs/GaAs QD grown by metalorganic chemical vapor deposition (MOCVD) (a) 1 μm × 1 μm AFM image; and (b), its PL spectra.
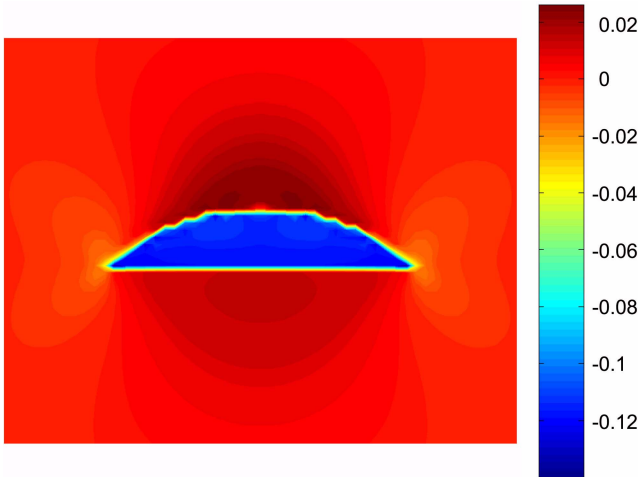
Fig. 2. In-plane strain ($e_{xx}+e_{yy}$) distribution of the InAs/GaAs QD (corresponds to structure (a) in the text).

Fig. 3. Interband transition spectra of the QDs in Fig. 2 with TE and TM polarized light.

optimization of each parameter characterizing QDs.

In this paper, we focus on the effects of the coupling among the QDs. As the surface density of self-assembled InGaAs quantum dots increases, it is not uncommon to observe island overlap where the QD wave functions laterally interact with each other. To investigate the effects of the quantum mechanical coupling, we calculate the electronic and optical properties of laterally coupled self-assembled quantum dots (SAQDs) using the eight-band $\mathbf{k}\cdot\mathbf{p}$ method. One of the most significant effects of the lateral coupling is an enhancement of the piezoelectric potential depending on the direction of the coupling[13]. In this paper, we focus on SAQDs configurations that enhance the positive piezoelectric potential; *i.e.*, laterally ([110]) coupled structure, and anti-correlated stacking structure. This paper is organized as follows: In Sec. 2, the numerical methods and the nanostructures investigated in this paper are described. The effects of

the coupling to electronic structures are presented in Sec. 3, and the optical properties are discussed in Sec. 4.

2. STRUCTURE MODEL AND COMPUTATIONAL METHODS

Figures 4(a) - (d) show the geometries of the four structures under investigation. Structure (a) (Fig. 4(a)) is a SQD with a diameter of 23.7 nm and a height 4.52 nm, which is used as a reference. Here, we used a lens-shaped QD which is more realistic than pyramidal and truncated pyramidal QDs. The major difference between the lens-shaped QD and (truncated) pyramidal QD is the magnitude of the piezoelectric potential. As dipoles are mainly located along the edges of a QD[14], the magnitude of the piezoelectric potential scales

(a)   (b)

(c)   (d)
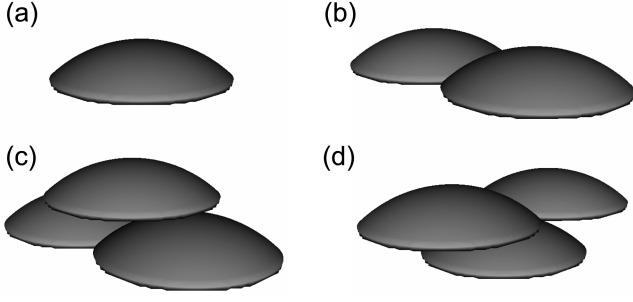
Fig. 4. Geometrical configurations of the QD structures. (a) SQD, (b) QDs coupled in the lateral ([110]) direction, (c) anti-correlated stacked structure (lower plane: LCQDs coupled along the [110] direction, upper plane: SQD, 1.13 nm above the lower plane), (d) anti-correlated stacked structure (lower plane: SQD, upper plane: LCQDs coupled to the [1$\bar{1}$0] direction, 1.13 nm above the lower plane).

with the size of the QD edge. As expected, the absence of sharp edges and corners in lens-shaped QDs results in a weaker piezoelectric potential (-21 meV to +26 meV) compared to truncated pyramidal QDs (-133 meV to +133 meV[13]). Structure (b) (Fig. 4(b)) shows laterally coupled quantum dots (LCQDs) coupled along the [110] direction (hereafter '[110] LCQDs'). As shown in a previous study[13, 15], the piezoelectric potential has $\mathbf{C_{2v}}$ symmetry, with positive potential on the dot edges in the [110] direction and negative potential on the dot edges in the [1$\bar{1}$0] direction. Thus, the positive piezoelectric potential is enhanced by the lateral coupling in the [110] direction up to 36 meV. Structure (c) is an anti-correlated structure that consists of [110] LCQDs in the lower plane and a SQD on the upper plane, while structure (d) is an anti-correlated structure that consists of [1$\bar{1}$0] LCQDs (LCQDs coupled along the [1$\bar{1}$0] direction) on the upper plane and SQD in the lower plane. The spacing between the upper and lower planes measures 1.13 nm. As the SQD in configurations (c) and (d) enhances the positive component of the piezoelectric potential and cancels part of its negative component[15], the conduction band (CB) coupling is enhanced while the valence band (VB) coupling is limited, as will be seen in Sec. 3.

We used the VFF method to calculate the strain of the coupled structures, and the eight-band $\mathbf{k \cdot p}$ method to obtain the electronic and optical properties of the structures. In VFF method, the strain energy is expressed in terms of the interatomic distances in order to determine the equilibrium atomic positions by minimizing the strain energy. The VFF method provides more accurate strain distributions than the continuum elasticity (CE) method, as it can treat the anharmonic effects important in systems with large lattice mismatches (7% for InAs/GaAs) and with rapidly varying strain distributions (usually observed in coupled QDs). Furthermore, unlike CE, which is based on bulk $\mathbf{C_{4v}}$ strain, VFF reproduces atomic positions in the $\mathbf{C_{2v}}$ symmetry of the

zincblende structure. This is especially important while comparing the anisotropy in the electronic and optical properties for QD coupling along the [110] and [1$\bar{1}$0] directions, as addressed in Sec. 3 and 4.

In the $\mathbf{k \cdot p}$ method, the electronic wave functions in the periodic lattice are expressed as Bloch wave functions,

$$\psi(r) = e^{ik \cdot r} u_{nk}(r) \qquad (1)$$

where, $\mathbf{u_{nk}}$ denotes the atomic-periodic part of the wave function, and $\mathbf{n}$ and $\mathbf{k}$ denote the band index and wavevector, respectively. The entire wave functions of the system can be considered as a linear combination of these basis functions.

$$\Psi(r) = \sum_{n,k} f_n e^{ik \cdot r} u_{nk}(r) = \sum_{n,k} F_n u_{nk}(r) \qquad (2)$$

Hence, the envelope $\mathbf{F}$ can be regarded as the amplitude of each basis function. Luttinger and Kohn[16] have proven that the summation over $\mathbf{k}$ can be left out, so the wave function becomes,

$$\Psi(r) = \sum_n F_n u_{nk_0}(r) \qquad (3)$$

where $\mathbf{k_0}$ denotes a fixed point in the Brilloine zone. In general, it is sufficient to use eight bands (two CB bands and six VB bands) near the fundamental gap explicitly, while the other (remote) bands are included by Löwdin's renormalization method[17]. Such truncation of the basis restricts the valid region of the $\mathbf{k \cdot p}$ method to the wavevector $\mathbf{k}$ in the vicinity (10 - 20%) of specific points (usually the Γ (k = 0) point for the optical transition) of the bulk band structure. However, as the size of ordinary QDs is much larger than that of single atoms, the $\mathbf{k \cdot p}$ method provides a very good agreement with experimental data.

3. ELECTRONIC STRUCTURE

Figures 5 and 6 show the CB and VB probability density of structures (a), (b), (c), and (d), respectively. In SQD, the CB and VB ground states have s-like symmetry and correspond to the '$|000\rangle$' state in the notations in Ref. [18]. The CB ground state is slightly elongated in the [110] direction, whereas the VB one is remarkably elongated in the [1$\bar{1}$0] direction[18]. The first and second excited states have p-like symmetry, and the third to fifth excited states have d-like symmetry. The energy splitting between the first and second excited states originates from the $\mathbf{C_{2v}}$ properties of the zincblende strain and the piezoelectric potential. The positive piezoelectric potential on the dot edges in the [110] direction lowers the energy of the state elongated in this direction, while the negative piezoelectric potential on the dot edges in the [1$\bar{1}$0] direction raises the energy of state elongated in that direction. As a result, the energy of the '$|100\rangle$' CB state (elongated in the [110] direction) is lower

than that of the '$|010\rangle$' CB state (elongated in the [$1\bar{1}0$] direction). On the opposite, in the VB, the first excited state is elongated along the [$1\bar{1}0$] direction and the second excited state is elongated along the [110] direction. In the coupled structures (Figs. 5(b) - 5(d)), the wave functions are strongly deformed by coupling, especially for higher excited states in the coupling region, where it is no longer possible to label each quantum state with only a single "quantum number"[18]. Instead, we identify each coupled state by attaching a bonding and anti-bonding label to the index of the SQD state. As the strain of two QDs are identical (Fig. 5(b)), their potential profiles are also identical. Accordingly, wave function coupling occurs between states with the same energy and the same "quantum number". The CB ground and first excited states in structure (b) are the bonding and anti-bonding states of the two ground (= $|000\rangle$) states in each quantum dot, and are labeled as '$|0+\rangle$'('+' denotes 'bonding') and '$|0-\rangle$'('-' denotes 'anti-bonding'), respectively. For simplicity's sake, we labeled the SQD ground state as '$|0\rangle$', the first excited state as '$|1\rangle$', with the pattern continuing. Similarly, the CB second to fifth excited states in structure (b) are labeled as '$|1+\rangle$', '$|2+\rangle$', '$|2-\rangle$' and '$|1-\rangle$', respectively. It is important to note that the energy of the '$|1-\rangle$' state is even higher than that of '$|2-\rangle$' as can be seen in Fig. 7. This is due to the fact that the wave function overlap between two CB '$|1\rangle$' states, which are elongated along the coupled direction in structure (b), is larger than that between two CB '$|2\rangle$' states, hence the bonding to anti-bonding splitting is larger in the coupled state of the CB '$|1\rangle$' compared to that of the CB '$|2\rangle$'. The magnitude of the wave function overlap in the coupling region is remarkably enhanced by the increased positive piezoelectric potential in that region. As a result, relatively large energy splitting (26.6 meV) is observed between the CB bonding ('$|1+\rangle$') and anti-bonding ('$|1-\rangle$') states. Conversely, in the VB, as the '$|2\rangle$' states are elongated along the [110] direction, the splitting between '$|2+\rangle$' and '$|2-\rangle$' is larger than that between '$|1+\rangle$' and '$|1-\rangle$'. As can be seen in Fig. 6(b), the VB ground and first excited states in structure (b) are localized in the coupling region. This is because, in structure (b), since two QDs are spatially overlapping and the compressive strain in the coupling region is weakened, the band gap of the coupled region is lower than that of the two QDs. However, such a localized VB state exists only for specific dot geometry and coupling conditions. As reported in a previous paper by the authors[13], in spite of the strong (- 0.2696 V) negative piezoelectric potential in the coupling region of the LCQDs linked in the [$1\bar{1}0$] direction, no localized VB state is observed at that region. For the (c) and (d) anti-correlated structures (Fig. 5(c) and 5(d)), we labeled each coupled state by a combination of states in structures (a) and (b). The subscript (superscript) denotes the state of the lower (upper) plane. The ground states of structure (c) are labeled as '$|_{0+}\rangle$', '$|_{0-}\rangle$'

(not shown in Fig. 5), where the superscript is omitted because no ground state exists on the upper plane (SQD). Although the distances between QDs in structures (c) and (d) are closer than that of experimentally observed anti-correlated structures[19], it was not possible to observe a coupling between the upper and lower planes in the ground state of these structures. On the contrary, the excited states show
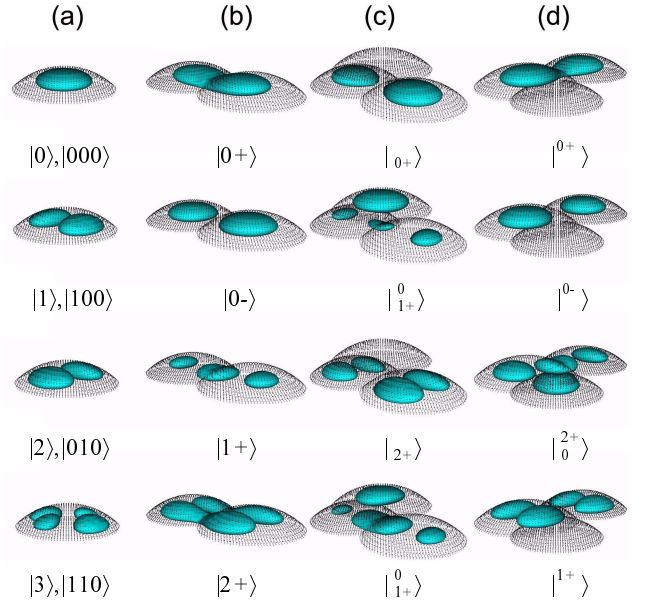
Fig. 5. Electron probability density for the ground to the third excited state. $|000\rangle$, $|100\rangle$, $|010\rangle$, and $|110\rangle$ represent the number of electron probability density nodes in the [110], [$1\bar{1}0$] and [001] directions[18]. For simplicity's sake, we labeled these states by $|0\rangle$, $|1\rangle$, $|2\rangle$ and $|3\rangle$. '+' ('−') denotes the bonding (anti-bonding) state. The subscript (superscript) in (c) and (d) denotes the state of the lower (upper) plane. See text.
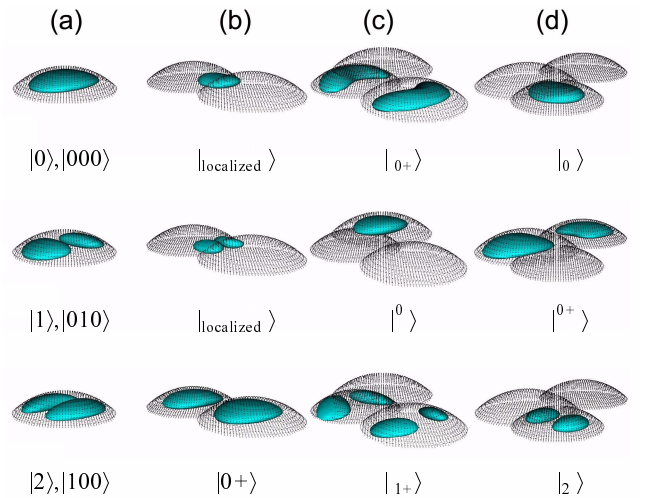

Fig. 6. Hole probability density in structures (a) – (d); the notations are identical to those in Fig. 5.
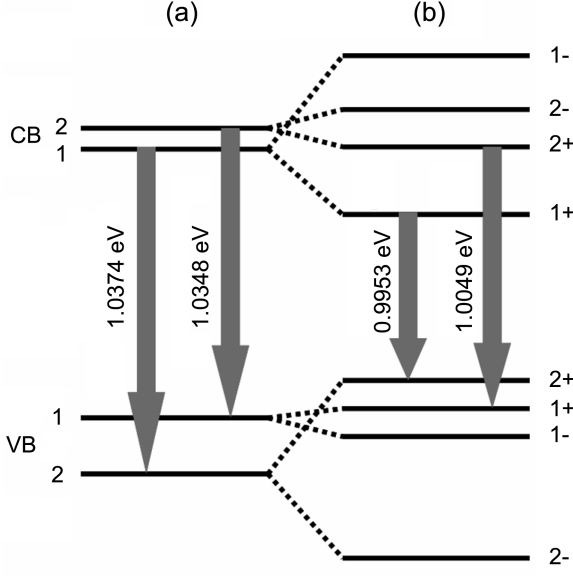
Fig. 7. Schematic of the energy spectra for the first and second excited states in structure (a), and the corresponding bonding and anti-bonding states in the coupled structure (b), with the first two optical transitions. The other transitions in (b) are very weak. The magnitude of the splitting depends on the orientation of each wave function. See text.

strong coupling, since the wave functions of the excited states are more extended toward the QDs boundary. The excited states are labeled as '$\left|{}^{0}_{1+}\right| +\rangle$', '$\left|{}_{2+}\rangle$', '$\left|{}^{0}_{1+}\right| -\rangle$', '$\left|{}_{2-}\rangle$', '$\left|{}^{1}_{1-}\rangle$', '$\left|{}^{2}_{4+}\rangle$' with this pattern continuing. Unlike the symmetric QDs in configuration (b), the three QDs in structures (c) and (d) have different strain and piezoelectric potentials. As the compressive strain is larger in SQD (upper plane of structure (c) and lower plane of structure (d)) compared to LCQDs (lower plane of structure (c) and upper plane of structure (d))[15], the energy of SQD is increased by the strong compressive strain compared to that of the LCQDs. As a result, coupling occurs between the LCQD higher state and the SQD lower state. The second ('$\left|{}^{0}_{1+}\right| +\rangle$') and fourth ('$\left|{}^{0}_{1+}\right| -\rangle$') excited states are the bonding and anti-bonding states of the '$\left|1+\rangle$' state on the lower plane and the '$\left|0\rangle$' state in the upper plane (without confusion, notations for distinguishing such 'mixed' bonding and anti-bonding states will be omitted hereafter. Both states will be denoted by the same '$\left|{}^{0}_{1+}\rangle$' symbol.). Due to the large overlap integral between the '$\left|1+\rangle$' state on the lower plane and the '$\left|0\rangle$' state in the upper plane, the two states are split by a large (22.9 meV) energy. Such mixed bonding and anti-bonding states are also observed in structure (d). As structures (b) - (d) intensify the positive piezoelectric potential in the coupling region, the VB coupling is weaker than the CB coupling due to the low hole probability density in the coupling region.
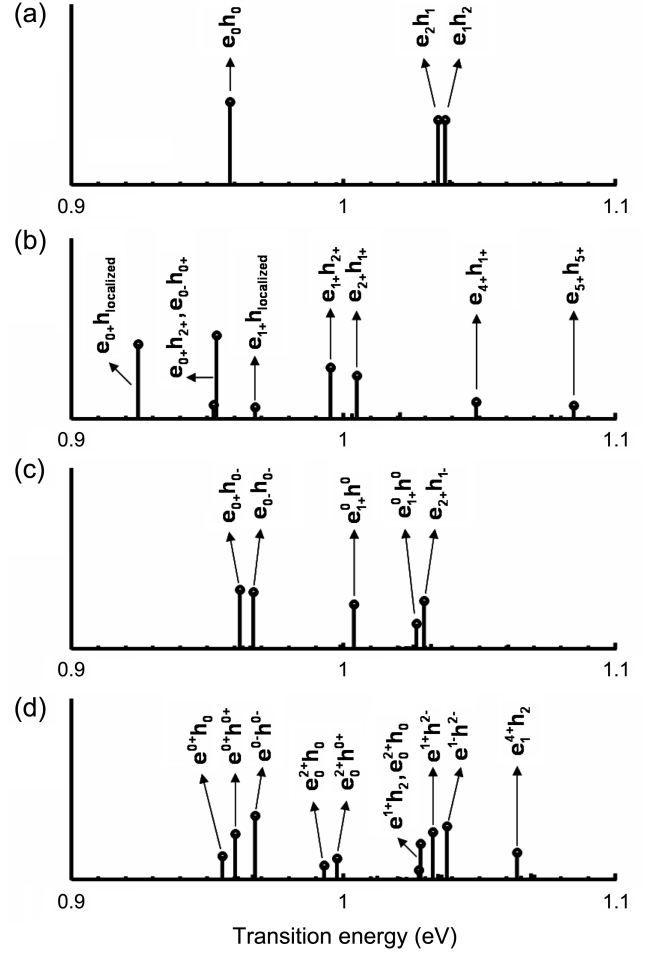
Fig. 8. Interband absorption spectra with TE polarization for the four structures.

4. OPTICAL PROPERTIES

Figure 8 shows the oscillator strengths for the interband transitions with TE polarized light for structures (a) - (d). Figure 8(a) shows the SQD transition spectra (structure (a)), where '$e_m h_n$' indicates a transition between the CB $|m\rangle$ state and the VB $|n\rangle$ state (Figs. 5 and 6). The oscillator strengths of the other transitions (e.g. $e_0 h_1$, $e_1 h_1$, $e_2 h_2$, ...) in the energy ranges shown in Fig. 8 are forbidden (very weak) due to selection rules. Similar to the result from pseudopotential calculation[7], the next allowed transitions are observed at 1.1104 eV, 1.1111 eV and 1.1136 eV, which correspond to $e_3 h_3$, $e_4 h_4$ and $e_5 h_5$ transitions (differences in the transition energies mainly arise from different QD geometry used in this work.), respectively. Figures 8(b) - (d) show the transition spectra of coupled structures ((b) - (d)), where we used the notations defined in Sec. 3 were used. $e_{0+} h_{localized}$ in Fig. 8(b) denotes a transition between the CB '$|0+\rangle$' state and the VB 'localized' (in the coupled region) state, $e_{0+} h_{2+}$ denotes a transition between the CB '$|0+\rangle$' state and the VB

'$|2+\rangle$' state, and $\mathbf{e}_{1+}^{0}\mathbf{h}^{0}$ in Fig. 8(c) corresponds to a transition between the CB '$|_{1+}^{0}\rangle$' state and the VB '$|^{0}\rangle$' state, continuing in this manner. The first peak ($\mathbf{e}_{0+}\mathbf{h}_{localized}$) in structure (b) shows a strong red shift (33.6 meV) compared to that of SQD (Fig. 8(a)). As the localized VB state exists only for specific coupling conditions, as reported in Sec. 3, such a large red shift is not a general property of LCQDs. In contrast, the red shifts of the next peaks ($\mathbf{e}_{0+}\mathbf{h}_{2+}$ and $\mathbf{e}_{0}\mathbf{h}_{0+}$, 4.8 meV red shift) are always expected in LCQDs (the magnitudes of red shifts depend on the coupling strengths), as the origin of these shifts are from weakened confinement conditions in the coupling region. The magnitude of the red shift is larger for the excited states ($\mathbf{e}_{1+}\mathbf{h}_{2+}$, $\mathbf{e}_{2+}\mathbf{h}_{1+}$), which are more extended toward the QD boundary, compared to the ground state ($\mathbf{e}_{0}.\mathbf{h}_{0+}$), which is almost localized inside the QD. It is interesting to note that the sequence (order) of the excited transitions in LCQDs is inverted compared to the SQDs. In the SQDs, the $\mathbf{e}_{2}\mathbf{h}_{1}$ transition energy is smaller than that of $\mathbf{e}_{1}\mathbf{h}_{2}$, while in LCQDs, the $\mathbf{e}_{1+}\mathbf{h}_{2+}$ transition energy is larger than that of $\mathbf{e}_{2+}\mathbf{h}_{1+}$. As shown in Sec. 3 and Fig. 7, this is explained by the stronger coupling between the '$|1\rangle$' states, which are elongated in the [110] LCQDs coupling direction, compared to that between the '$|2\rangle$' states.

The first two ground peaks in structure (c) show small blue shifts (3.8 meV and 8.7 meV) compared to those in the SQD, while the fifth peak ($\mathbf{e}_{2+}\mathbf{h}_{1-}$) shows a red shift (5.1 meV) compared to $\mathbf{e}_{2}\mathbf{h}_{1}$ in the SQD. The blue shifts of the first two ground peaks originate from the enhanced compressive strain in the QDs, while the red shift of the $\mathbf{e}_{2+}\mathbf{h}_{1-}$ peak originates from the weakened confinement condition in the coupling region. As the excited states are more extended toward the QD boundary than the ground state, the red shifts from the weakened confinement exceed the blue shifts by the enhanced compressive strain. Transitions $\mathbf{e}_{1+}^{0}\mathbf{h}^{0}$ (mixed bonding $\mathbf{e}_{1+}^{0}$) and $\mathbf{e}_{1+}^{0}\mathbf{h}^{0}$ (mixed anti-bonding $\mathbf{e}_{1+}^{0}$) have no counterparts in the SQD spectra, as these peaks result from transitions involving mixed states ('$|_{1+}^{0}\rangle$', Fig. 5(c)). The splitting between these two peaks is relatively large (22.9 meV) due to the large overlap integral between the upper and lower planes, as seen in Sec. 3. In structure (d) (Fig. 5(d)), the lowest peaks ($\mathbf{e}^{0+}\mathbf{h}_{0}$, $\mathbf{e}^{0+}\mathbf{h}^{0+}$, $\mathbf{e}^{0}\mathbf{h}^{0-}$) show blue shifts compared to the lower transition of the SQD, and the transitions $\mathbf{e}^{1+}\mathbf{h}^{2-}$, $\mathbf{e}^{1-}\mathbf{h}^{2-}$ have almost the same energies as their counterparts in the SQD spectra ($\mathbf{e}_{2}\mathbf{h}_{1}$, $\mathbf{e}_{1}\mathbf{h}_{2}$). This results as the blue shifts arising from enhanced compressive strain and the red shifts resulting from weakened confinement compensate each other in the excited states ($\mathbf{e}^{1+}\mathbf{h}^{2-}$, $\mathbf{e}^{1-}\mathbf{h}^{2-}$) of structure (d). Similar to structure (c), transitions involving mixed states ($\mathbf{e}_{0}^{2+}\mathbf{h}_{0}$ (mixed bonding $\mathbf{e}_{0}^{2+}$), $\mathbf{e}_{0}^{2+}\mathbf{h}^{0+}$ (mixed bonding $\mathbf{e}_{0}^{2+}$) and $\mathbf{e}_{0}^{2+}\mathbf{h}_{0}$ (mixed anti-bonding $\mathbf{e}_{0}^{2+}$)) are observed in structure (d) as well. Moreover, a large amount of energy splitting (35.6 meV) is observed for mixed bonding and anti-bonding peaks of $\mathbf{e}_{0}^{2+}\mathbf{h}^{0+}$ by the large wave function overlap between the upper and lower planes.

5. CONCLUSIONS

We have investigated the effects of wave function coupling in two types of SAQDs configurations: (i) laterally ([110]) coupled structure and (ii) anti-correlated stacking structure, by using an eight-bands $\mathbf{k}\cdot\mathbf{p}$ method. The wave functions of coupled structures are strongly deformed, thus we identify the wave functions by their counterparts in the SQD. Unlike in LCQDs, which are characterized by symmetric coupling between the two QDs wave functions, the QDs on the upper and lower planes of the anti-correlated structures have asymmetric configurations, hence coupling occurs between different states belonging to those two planes (mixed coupling). Moreover, we obtained highly localized VB states in the LCQD coupling region. A transition involving such a localized VB state shows a large red shift compared to that of the SQD. Inversions in the order of excited transitions are observed in LCQDs ($\mathbf{e}_{1+}\mathbf{h}_{2+}$, $\mathbf{e}_{2+}\mathbf{h}_{1+}$) compared to SQD ($\mathbf{e}_{2}\mathbf{h}_{1}$, $\mathbf{e}_{1}\mathbf{h}_{2}$). This is explained by the differences in the wave function overlap between the two '$|1\rangle$' states and the two '$|2\rangle$' states. In addition, the origin of spectral shift in the anti-correlated structures, which involves mixed states, was interpreted in terms of the strain and confinement conditions in the coupled QDs.

ACKNOWLEDGEMENTS

REFERENCES

1. Q. Gong, R. Nötzel, P. J. van Veldhoven, T. J. Eijkemans, and J. H. Wolter, *Appl. Phys. Lett.* **84**, 275 (2004).
2. M. Sugawara, T. Akiyama, N. Hatori, Y. Nakata, H. Ebe, and H. Ishikawa, *Meas. Sci. Technol.* **13**, 1683 (2002).
3. R. Hanson, L. M. K. Vandersypen, L. H. Willems van Beveren, J. M. Elzerman, I. T. Vink, and L. P. Kouwenhoven, *Phys. Rev. B* **70**, 241304 (2004).
4. X. Li, Y. Wu, D. Steel, D. Gammon, T. H. Stievater, D. S. Katzer, D. Park, C. Piermarocchi, and L. J. Sham, *Science* **301**, 809 (2003).
5. Y. Lee, E. Ahn, P. Moon, J. Kim, C. Yang, E. Yoon, H. Lim, and H. Cheong, in preparing.
6. C. Pryor, J. Kim, L. W. Wang, A. J. Williamson, and A. Zunger, *J. Appl. Phys.* **83**, 2548 (1998).
7. J. Shumway, A. J. Williamson, A. Zunger, A. Passaseo, M. DeGiorgi, R. Cingolani, M. Catalano, and P. Crozier, *Phys. Rev. B* **64**, 125302 (2001).

8. W. Sheng and J.-P. Leburton, *Phys. Rev. B* **64**, 153302 (2001).

9. N. K. Cho, S. P. Ryu, J. D. Song, W. J. Choi, J. I. Lee, and H. Jeon, *Appl. Phys. Lett.* **88**, 133104 (2006).

10. J. A. Barker and E. P. O'Reilly, *Phys. Rev. B* **61**, 13840 (2000).

11. K. Park, P. Moon, E. Ahn, S. Hong, E. Yoon, J. W. Yoon, H. Cheong, and J.-P. Leburton, *Appl. Phys. Lett.* **86**, 223110 (2005).

12. F. Guffarth, R. Heitz, A. Schliwa, O. Stier, N. N. Ledentsov, A. R. Kovsh, V. M. Ustinov, and D. Bimberg, *Phys. Rev. B* **64**, 085305 (2001).

13. P. Moon, W. Sheng, E. Yoon, and J.-P. Leburton, in preparation.

14. M. Grundmann, O. Stier, and D. Bimberg, *Phys. Rev. B* **52**, 11969 (1995).

15. P. Moon, E. Yoon, and J.-P. Leburton, *Proceedings of 2005 5th IEEE Conference on Nanotechnology,* Nagoya, Japan (2005).

16. J. M. Luttinger and W. Kohn, *Phys. Rev.* **97**, 869 (1954).

17. S. L. Chuang, *Physics of Optoelectronic Devices,* Wiley-Interscience, NY (1995).

18. O. Stier, M. Grundmann, and D. Bimberg, *Phys. Rev. B* **59**, 5688 (1998).

19. X. -D. Wang, N. Liu, C. K. Shih, S. Govindaraju, and A. L. Holmes, Jr., *Appl. Phys. Lett.* **85**, 1356 (2004).